Reservoir characterisation and numerical modelling to reduce project risk and maximise the chance of success. An example of how to design a stimulation program and assess fluid production from the Soultz geothermal field, France

Joshua Koh[1], Nima Gholizadeh-Doonechaly[1], Abdul Ravoof[1] and Sheik S Rahman*[1], Luke Mortimer[2]
[1]School of Petroleum Engineering, University of New South Wales, Sydney
[2]Hot Dry Rocks Pty Ltd, 1A Yarra Street, South Yarra, Victoria

This paper describes a predictive, fully coupled poro-thermo-elastic numerical model that is specifically developed to evaluate and optimise geothermal reservoir development strategies. This paper illustrates this via an investigation into the role of stimulation to enhance the permeability for economic hot water production from the deep geothermal site at Soultz-sous-Foréts (France). This study integrates four key elements: a natural fracture characterization model, a fluid flow simulation model, a heat transfer model and a stimulation model. Fluid flow is simulated using a finite element based model wherein stresses and temperature are fully coupled to the fluid flow equations. The heat transfer model is based on conductive heat transfer within the reservoir rock, convective (including conduction) heat transfer through the reservoir fluid and time dependent thermal equilibrium between the rock and fluid. The stimulation model integrates shear dilation mechanisms and stress dependent permeabilities. Effective permeability tensors (based on discrete fracture network) are estimated dynamically and are iteratively used to determine the pore pressure, stress and thermal state within the reservoir.

A numerical reservoir model of the Soultz-sous-Foréts field was constructed based on the data available in the open literature. The reservoir was subjected to different pressure cycles to determine the degree of permeability enhancement that could be achieved. Flow rate and corresponding pressure losses between injector and producers as well as heat recovery of the produced water were calculated to assess the geothermal potential of the reservoir. Results of this study show that effective tensile normal stresses from the injected cold fluid tend to increase fracture apertures, and hence, increase fracture permeability within the zone of cooling. It was also shown that for a nominal stimulation bottomhole pressure of 10,000 psi, a maximum number of shear dilation events is observed after a stimulation period of 42 weeks for the generated Soultz fracture system and this level of stimulation was sufficient to obtain an economic flow rate of 100 L/s (at an acceptable pressure loss of 2000psi). Our experience also shows that prior to stimulation, flow rates at an acceptable pressure loss between the injector and producers are not sufficient for economic heat extraction. Hence these reservoirs require either stimulation to enhance reservoir permeability or installation of down-hole pumps to lift hot water.

In addition, it has been observed that a major factor responsible for heat recovery as well as thermal drawdown is the degree of interconnection of the fractured reservoir. The produced fluid temperature for the more weakly connected well GPK4 remains very high (~195^0 C) after a production period of 14 years. During the same period the average matrix temperature drawdown is in the order of 20^0 C for an initial reservoir temperature of 200^0C. For the case of a highly interconnected GPK2 well, the

temperature of the produced fluid falls from an initial temperature of 200^{0}C to about 130^{0}C after 14 years of production.

Introduction

Understanding of the hydraulic flow and heat transfer within crystalline rocks is of significant importance in the utilization of deep earth (at least 4 km) hot rock (HR) for geothermal reservoir systems (Baria et al. 1999; O'Sullivan et al. 2001). The characteristics of fluid flow and heat transfer in crystalline rocks are dominated by the fracture systems found within them and in-situ stress which affect the properties of the fracture system significantly. Modelling of coupled hydraulic, thermal and mechanical processes can help in the understanding of the effects of *in-situ* stresses, induced fluid pressure and heat transfer on fluid flow and thermal drawdown of naturally fractured geothermal systems. The long-term response of fracture systems to changes in effective stresses has been investigated by several authors (McDermott and Kolditz, 2006). The change in effective stresses can be induced by hydraulic and thermo-elastic stress alterations resulting from heat extraction from the fractured geothermal systems (rocks). Circulation of cold fluid induces temperature differences within the rock matrix due to heat transfer which leads to large amounts of stress energy release. In an experimental study, O'Sullivan et al (2001) observed some degree of geo-mechanical effects of thermal stresses on geothermal reservoir characteristics (fracture apertures and fracture permeability) and suggested a need for a long term investigation of the thermal stress effect. In particular, the mechanisms that cause phenomena, such as variation of injectivity/productivity with thermal drawdown and occurrence of seismicity need to be understood.

The response of a fracture network to stimulation by injection of cool fluid is time dependent and is a function of discrete fracture behaviour (McDermott et al. 2006; Beeler and Hickman 2003). The individual response of the discrete fractures within the fracture system are determined by interaction of the injected fluid and its physical characteristics such as viscosity, heat capacity and temperature. Other factors, such as the elastic response of the rock matrix and pervasive *in-situ* conditions, including pore pressure and rock temperature have a significant bearing on the closure and shear state of a fracture. The effective stress profiles along fracture surfaces are functions of the far field tectonic stresses, induced hydraulic stresses and thermal stress release (McDermott et al. 2006) during heat extraction. Induced tensile stresses normal to the fracture surfaces from cold water injection can increase fracture aperture and induce new fractures (Zhou et al., 2009). Therefore, alterations of fracture system parameters, such as effective permeability need to be coupled to changes in the pervasive conditions.

Recently, Rutqvist and Stephanson (2003) provided a generic overview of models used for hydromechanical coupling at an aquifer depth and a number of well-known empirical approaches to changes in the normal stress across fractured medium. Most notable, is the study by Beeler et al (2000) who applied elastic solutions for elliptical cracks to define the deformation responses of elliptical fractures under tectonic loading. The effect on the surrounding rock mass however, was not included.

Few authors have investigated the effects of induced fluid pressure on naturally fractured rock on a reservoir scale. Rahman et al. (2002) developed a steady state fluid flow model to study the shear dilation effect due to fluid pressure on permeability enhancement. Shaik et al. (2009) considered poroelastic stresses in the stimulation of a discrete fracture network by induced fluid pressure. In the aforementioned studies, however, thermal stresses were not considered.

Kumar and Ghassemi (2005) developed a numerical model to study fluid pressure and permeability changes in a rock mass by taking into account the effects of thermal stresses and silica precipitation/dissolution. The numerical model incorporated a single planar fracture connecting an injection well and a production well as an idealized reservoir-matrix system. The temporal variation of fracture aperture in response to the individual and combined effects of thermo-elastic stress and silica dissolution/precipitation were examined, however, changes in fracture aperture and pressure in response to non-uniform cooling were not addressed.

Poroelastic and thermoelastic effects of cold-water injection into a single pre-existing fracture in a hot rock matrix was investigated by Ghassemi et al. (2007). Assumptions of plane fracture geometry were used to derive expressions for changes in fracture aperture caused by cooling and fluid leak-off into the matrix. The variations in aperture and pressure occurring under non-isothermal flow conditions when the fracture is subject to injection and heat extraction were examined. The problem was analytically solved for the cases pertaining to a constant fluid injection rate with a constant leak-off rate using a partially coupled formulation.

As part of this study, four computationally efficient models are presented in an effort to evaluate and optimise reservoir development strategies: a natural fracture characterization model, a fluid flow simulation model, a heat transfer model and a stimulation model. The fully coupled thermo-poroelastic numerical model is applied to the Soultz geothermal reservoir, France, where several deep wells have been drilled and stimulated in the Rhine graben (Soultz, France) to evaluate the geothermal Hot Dry Rock potential of the deep fractured granite reservoir. Three main boreholes, GPK2, GPK3 and GPK4 which reach 5080, 5100 and 5270m depth respectively, intersect a crystalline basement overlain by 1400m of Cenozoic and Mesozoic sediments. The layout of the Soultz-sous-Forets EGS site and the well traces and locations are presented in **Fig. 1**. The novelty of this approach lies in its dynamic treatment of the characteristic properties of individual fractures in simulating fluid flow and the pervasive response of the natural fracture system to cold fluid injection. The coupled numerical algorithm is presented in **Fig. 2**.

Modelling of the Soultz fracture network

Variably oriented and intersected fractures with different sizes and irregular patterns (i.e. all fracture complexities) are characterized with the use of two integrated methodologies (Tran, Chen et al. 2007). In the hybrid neuro stochastic methodology, fracture properties are generated based on their characterized statistical distributions. A selective random sampling scheme is used for this purpose. Continuum maps of fracture density and multifractal dimensions are integrated in the discrete model. Hierarchical simulation technique is used to deal with different degrees of heterogeneity in the

reservoir. In the second methodology, hybrid neuro stochastic methodology is upgraded to handle more complex measurements. In this methodology, an object based conditional global optimization concept is applied. It combines continuum distributions with statistical distributions and correlations of discrete fracture properties, thus representing a great improvement over other object based stochastic simulation as well as grid based fracture models.

Based on the observed data recorded, a specified number (say 1000 fractures) of unbiased data specimens are generated by re-sampling the weighting field using a normalized probability method for different fracture classes. Once at least 1000 fractures are created, then the fractures are sorted with respect to their radii. The sorting is performed based on the input value for the smallest and the largest fractures to be modeled. Once the fracture network with specific characteristics is generated, the next step is to define the fracture density in a square volume of rock of interest. The fracture density is the representation of the fracture area per unit volume of rock mass observed in the field. The fracture network is stochastically realized within this volume using a pseudo-random number generator. This is accomplished by repeated re-sampling of earlier fracture records and placing the fractures randomly in the volume of interest until the required fracture density is reached.

In this study, the statistical analysis of the fracture networks in the Soultz geothermal reservoir as performed by Gentier et al. (2010) was used. **Table 1** presents the four main fracture sets F1, F2, F3 and F4, with a fifth set F5 defined for fractures not falling within the initial four main sets as "background noise" (Gentier et al., 2010). Two ~N-S striking sets are distinctly recognised, respectively W-dipping (F1) and ENE-dipping (F2). In addition, two NE-SW and NW-SE striking sets are also observed, respectively NW-dipping (F3) and SW-dipping (F4).

The fracture data was used to stochastically resample the fracture network around the wells GPK2, GPK3 and GPK4 in the abovementioned manner. The generated fracture network is presented in **Fig. 3** for a parallelepiped volume of 2.5 km (east west) by 3.0 km (north south) by 3.5 km (vertical, 2500m – 6000m).

Numerical flow simulation

A finite element based poro-thermo-elastic reservoir model is developed for evaluating hot water production. This model fully couples fluid flow, temperature and geomechanics. The governing equations of non-isothermal thermo-poroelasticity is expressed as follows (Kurashige, 1989; Ghassemi et al., 2002):

$$\left(K+\frac{G}{3}\right)\nabla(\nabla\cdot u)+G\nabla^2 u-\alpha\nabla p-\gamma_1\nabla T_R=0 \tag{0.1}$$

$$\frac{\partial\zeta}{\partial t}=\frac{k}{\mu}\nabla^2 p \tag{0.2}$$

$$\dot{\zeta}=\alpha\dot{\varepsilon}_{ii}+Q'\dot{p}-\gamma_2\dot{T} \tag{1.3}$$

$$\dot{T}_f+\nabla(J_f T_f)-{c_f}^T\nabla^2 T_f=0 \tag{1.4}$$

$$\dot{T}_R - c_R{}^T \nabla^2 T_R = 0 \tag{1.5}$$

where, K is the bulk modulus (MPa), G is the shear modulus (MPa), u is the displacement vector, (ux, uy) (m), α is Biot's coefficient, γ_1 is the thermal expansion coefficient of solid (K^{-1}), γ_2 is the thermal expansion coefficient of fluid (K^{-1}), T_R and T_f are the rock and fluid temperatures respectively (K), p is the pore pressure (Pa). Superconvergent patch recovery (Zienkiewicz et al. 1992) is used to evaluate nodal stress tensors from the numerical results of nodal displacement, u.

Fracture response to stimulation

The naturally fractured medium is pressurised by injecting fluid with a view to stimulate the reservoir. In practice, the fluid pressure develops gradually and some of the fractures may start propagating before the fluid pressure reaches a threshold level at which shear slippage may takes place for a large number of fractures.

The shear slippage criterion similar to Rahman et.al (2000) is applied to identify fractures that are favorable for shear slippage and dilation. When the fracture pressure becomes higher than the given in-situ stress effective normal stress becomes negative and fractures open and surfaces no longer remain in contact. The shear displacement, U_s in such condition can be expressed as:

$$U_s = \frac{\tau_n}{K_s} \tag{1.6}$$

where K_s is the fracture shear stiffness and τ_n is the access shear stress.

The increase in fracture aperture due to shear dilation, a_s can be expressed as (Willis-Richards, Watanabe et al. 1996):

$$a_s = U_s \, tan(\varphi_{dil}^{eff}) \tag{1.7}$$

The total stimulated aperture can be expressed as (Muskat 1937):

$$a = \frac{a_0}{1 + 9\sigma_{eff} / \sigma_{nref}} + a_s + a_{res} \tag{1.8}$$

where a_{res} is the residual aperture that usually exists at high effective stress and is considered to be zero in this study. The normal effective stress, σ_{eff}, is the resultant normal stress arising from the effects of induced pressure and thermal contraction at the fracture surface. The total stimulated aperture, a can finally be expressed by mathematical manipulation as:

$$a = \frac{a_0 + U_s \, tan(\varphi_{dil})}{1 + 9\sigma_{eff} / \sigma_{nref}} \tag{1.9}$$

The above equation is used in the evaluation of permeability enhancement by numerical simulation of fluid flow within the stimulated fractured network.

Numerical algorithm

The algorithm of the design methodology is shown in Fig. 2. Initially, real field data, such as the fracture orientation, size and other fracture parameters that influence reservoir performance are acquired from the open literature.

An analysis of hot water productivity in terms of well placement is performed for three well configurations. Well location and distance between wells are chosen based on the Soultz EGS system and used to investigate common problems associated with development of EGS, such as short circuiting and high pressure loss between injector and producer wells, and at the same time a perform a hydraulic stimulation program to provide sufficient permeability enhancement.

For the configuration, the reservoir permeability is calculated based on the discrete fracture network data and fluid flow simulation. Then the injector is pressurised and the pore pressure, temperature and stress tensor across the reservoir at each time step are evaluated. Shear slippage and dilation that may occur as a result of change in local stress and pore pressure are determined and evaluated.

Numerical results of stress and pore pressure are used to calculate current total aperture (accounting for the contributions of fracture opening (mode I), shear dilation (mode II)) for every individual natural fracture and update the permeability of the reservoir.

Using these results, reservoir simulation is carried out to calculate flow rates at the producers for discrete values of injector-producer pressure drops as well as temperature profiles of both the rock and fluid within the reservoir.

Results and Discussion

In the current thermo-poroelastic numerical model, flow between the injection well and production wells are assumed to be planar and is approximated through the open hole interval (3500m to 5100m) through a statistically representative trace. This is achieved by alteration of the fractal dimension, which is used to spatially distribute the fractures within a defined volume. A statistically representative trace of the Soultz fracture network between a depth of 2500 m and 6000 m is presented in **Fig. 4**. The well placements on the plane are taken as their separation at a depth of 4430m, which is midway through their depth-averaged open hole sections. The reservoir is pressurized by injecting fluid through the injection well (GPK2). To increase the injectivity, a pair of co-planar fractures of half length of 30m, is placed at the injection well. The pressurization was carried out over a period of one year and the results recorded at different stages (8 weeks, 24 weeks, 40 weeks and 52 weeks). During the pressurization, the change in fracture width for each individual natural fracture and the resulting permeability tensor were calculated. Following stimulation of the reservoir, a flow test was carried out over a period of 14 years. During the flow test, changes in fracture apertures due to thermo-poro-elastic stresses and the consequent changes in permeabilities were determined. Also estimated was the thermal drawdown of the Soultz EGS.

Effect of stimulation time on shear dilation

Results of shear dilation are presented as average percentage increase in fracture aperture and dilation events with time (see **Figs. 5** and **6a-6d**). From Fig. 5, it can be seen that there exists three distinct aperture histories: 0-28 weeks, 28-42 weeks and greater than 42 weeks. Until about 28 weeks, the rate of occurrence of dilation events due to induced fluid pressure of 10,000 psi (bottomhole) remains fairly constant. Following this time, the rate of occurrence increases sharply until about 42 weeks, after which, no significant dilation events can be observed (a plateau of events is reached). This infers that for every set of reservoir and stress parameters as well as injection schedule, a maximum level of shear dilation can be achieved.

In Figs. 6a, 6b, 6c and 6d, the events of shear dilation at different stimulation times are presented. From these figures, it can be seen that by 8 weeks, distribution of shear dilation events is relatively non-uniform. This can be attributed to rapid propagation of pressure through well interconnected fractures.

As pressure continues to build up, more fractures are dilated in the vicinity of the active shear dilation front (see Figs. 6c and 6d). In **Fig. 7**, permeability enhancement in the form of the root mean square (RMS) permeability tensor, at the end of 16 weeks and 42 weeks of stimulation, respectively, are presented. The low initial permeabilities can be attributed to high *in situ* closure stresses in the reservoir. After 42 weeks of stimulation, reservoir permeability has been significantly increased, both due to pressure induced inflation (temporary) and shear dilation (retainable) of the fracture network. The RMS permeabilities local to the major fractures are roughly an order of magnitude greater after 42 weeks of stimulation than after 16 weeks.

Effect of well placement on reservoir stimulation and hot water production

As shown in Fig. 4, the two production wells, GPK2 and GPK4 are separated from the injection well, GPK3, by roughly 480m and 440m respectively. During stimulation, the production wells are kept closed. Once a desired stimulation is achieved at the end of the stimulation period (42 weeks) the fluid was circulated over a period of 14 years. During this circulation period, production rates from each well, fluid velocities throughout the reservoir produced fluid temperatures and average matrix temperature drawdown were estimated. The production parameters are listed in Table 2. Results of hot water production over the 14 year circulation period after an initial 42 weeks of stimulation are presented in **Figs. 8** through **13**.

In Fig. 8, the RMS fluid velocities after 10 years of production are presented. It can be observed from this figure that there exists distinct fluid flow paths connecting the injector and the producers. The flow paths connecting the injector and GPK4 however, are not as prominent (not well connected) as that of GPK2. In addition, it can be observed that the fluid velocities are much greater for the 42 week stimulation case than the 16 week stimulation case. Fluid velocities up to 1×10^{-3} m/s through the major connected pathways is reached after 42 weeks which is three times higher than that after 16 weeks of stimulation. In **Fig. 9**, the reservoir temperature profile after 10 years of production is presented. It is apparent from the figure that the high flow rates experienced between the injector and

producers (see Fig. 8) resulted in significant cooling of the reservoir rock along these flow paths. Once thermal breakthrough has taken place through to GPK2, the temperature of the produced fluid begins to decline steadily. This thermal breakthrough takes place at about 8 years of production (see **Fig. 10**). From Fig. 10, it can also be observed that the produced fluid temperature drops to about 140^{o}C in well GPK2, while in well GPK4, the produced fluid temperature remains high after the same period. The variation of produced fluid temperature from different wells is caused by several factors, namely, the number of hydraulically active flow paths between the injector and producer, the hydraulic length of these flow paths and the temperature difference between invading fluid and rock matrix along these flow paths. In general, a high number of flow paths originating from the injector, which span considerable distances before intersecting the producers, tends to delay the onset of thermal breakthrough (due a high heat-sweep efficiency). It may be noted from Fig. 10 that thermal breakthrough begins to occur at GPK4 at around 11 years.

Effect of thermally induced stresses on hot water production

In **Figs. 11a** and **11b**, the estimated reservoir impedances for two different degrees of stimulation are presented. Stage I stimulation (Fig. 11a) is over 26 weeks and stage II stimulation (Fig. 11b) over 42 weeks. As shown in Fig. 11b, the production rates at GPK2 increase rapidly for roughly one year and continue to increase but at a slower rate until about 8 years. Following this, a quasi steady state production with fluctuations is reached. The initial production period of one year is characterized by a steep increase in production rate as pressure builds up through the well connected network of stimulated fractures. The steady increase in production after one year can be attributed to the cooling of the rock matrix which induces thermal stresses (see **Figs. 12a** and **12b**). These thermal stresses consequently increase permeability of the fractured network, leading to changes in the pressure distribution and hence, the flow rates.

The effective stresses in the reservoir rock at early production time (3 years) and late production time (10 years) are presented in **Figs. 12a** (x direction) and **12b** (y direction). It should be noted again that a geomechanics sign convention is adopted for stresses (positive for compression). From both plots, it is apparent that the effective stresses in reservoir at late time (10 years) are significantly less compressive than those at early time. The decreases in effective stresses causes fracture dilation and therefore permeability enhancement. The continuous decrease in matrix temperature at an increasing rate can be observed in **Fig. 13**.

Effect of level of stimulation on reservoir impedance

The production flow rates at GPK2 were recorded for injector-producer pressure drops of 2000 psi and 1500 psi, for both stage I and II of stimulation. In Fig. 11a for the case of stage I stimulation, the production rates rise with time, until roughly 1.5 years, when a quasi-steady state pressure profile is attained. At this point, a 2000 psi pressure drop results in a production rate of roughly 30L/s while a 1500 psi pressure drop, roughly 16 L/s. Following this, the production rates continue to rise but at a much slower rate which was explained in the previous section. Peak production of 43 L/s is observed with a pressure drop of 2000 psi and 23 L/s with a pressure drop of 1500 psi.

In Fig. 11b, the production rate as a function of time after 42 weeks of stimulation is presented. It can be seen that the production rates with injector-producer pressure drops of 2000 psi and 1500 psi bear a similar trend to the case of stage I stimulation. The production rates begin to reach quasi-steady state (as observed in Fig. 11b) at around 1 year production time. Similarly, thermally induced stresses increase the production rates after this period for both cases of pressure drop. The production rate with a pressure drop of 2000 psi peaks around 100 L/s and around 63 L/s with a pressure drop of 1500 psi. The increased production rates were achieved by increasing the stimulation time from 26 weeks to 42 weeks.

Conclusions

In this paper, a poro-thermo-elastic reservoir model is developed and used to study the effects of induced fluid pressure and thermal stresses (cooling effect) on reservoir permeability and consequent increase in hot water production. The model is applied to the Soultz geothermal reservoir, France. The paper also investigates the effect of well placement on hot water production and thermal drawdown. From the results of this study, the following conclusions can be drawn.

It has been shown that for every geothermal system there exists an optimum injection schedule (injection pressure and duration). Further increases in stimulation effort, i.e. stimulation time for a given stimulation pressure, does not enhance any further reservoir permeability. In this study, for a bottomhole stimulation pressure of 10,000 psi, a stimulation time of 42 weeks has been found optimum.

Fracture connectivity has a significant bearing on thermal breakthrough, produced hot water temperature, temperature drawdown and the hot water production rate. Also demonstrated, was the non-uniform spatial distribution of shear event occurrences with time.

Thermal stresses induced during the circulation of cold water have a significant effect on the long term production rate. As thermal drawdown of the rock matrix takes place, tensile thermal stresses are induced which allow residing fractures to dilate and enhance permeability. This gradually increases the fluid velocities between the injector and producer, yielding increasing production rates with time.

References

Baria, R., Baumg¨artner, J., G´erard, A., Jung, R., Garnish, J., 1999. European HDR research programme at Soultz-sous-Forˆets (France) 1987–1996. Geothermics 28, 655–669.

Beeler, N. M., Wong, T. F. & Hickman, S. H., 2003. On the expected relationships among apparent stress, static stress drop, effective shear fracture energy, and efficiency. Bull. Seismol. Soc. Am. 93, 1381-1389.

Beeler, N.M., Simpson, R.W., Hickman, S.H. and Lockner, D.A., 2000. Pore fluid pressure, apparent friction, and Coulomb failure, J. Geophys. Res. 105, 25533– 25542.

Gentier, S., Rachez, X., Ngoc, T. D. T., Peter-Borie, M. and Souque, C. (2010). "3D Flow Modelling of the Medium-Term Circulation Test Performed in the Deep Geothermal Site of Soultz-Sous-forets (France). Proceedings Worlf Geothermal Congress 2010 - Bali, Indonesia, 25-29 April 2010.

Ghassemi, A. and G. Suresh Kumar (2007). "Changes in fracture aperture and fluid pressure due to thermal stress and silica dissolution/precipitation induced by heat extraction from subsurface rocks." Geothermics **36**(2): 115-140.

Ghassemi, A., Nygren, A., Cheng, A., 2008. Effects of heat extraction on fracture aperture:A poro–thermoelastic analysis. Geothermics 37, 525–539.

Jing, Z., J. Willis-Richards, et al. (2000). "A three-dimensional stochastic rock mechanics model of engineered geothermal systems in fractured crystalline rock." J. Geophys. Res. **105**.

Kumar, G.S. and Ghassemi, A., 2005. Numerical modeling of non-isothermal quartz dissolution/precipitation in a coupled fracture–matrix system. Geothermics 34 (2005) 411–439.

McDermott, C.I. and Kolditz, O., 2006. Geomechanical model for fracture deformation under hydraulic, mechanical and thermal loads. Hydrogeol. J. 14, 487–498.

Muskat, M. (1937). The Flow of Homogeneous Fluids Through Porous Media, Edwards Publisher.

Narayan, S. P., Z. Yang, et al. (1998). HDR reservoir development by fluid induced shear dilation: A numerical study of the Soultz and the Cooper Basin granite rock. International Hot Dry Rock - Forum, Strasbourg, France.

O'Sullivan, M.J., Pruess, K., Lippmann, M.J., 2001. Geothermal reservoir simulation. The state of practice and emerging trends. Geothermics 30 (4), 395–429.

Rahman, M. K., M. M. Hossain, et al. (2000). "An analytical method for mixed-mode propagation of pressurized fractures in remotely compressed rocks." International Journal of Fracture **103**(3): 243-258.

Rahman, M. K., M. M. Hossain, et al. (2002). "A Shear-Dilation-Based Model for Evaluation of Hydraulically Stimulated Naturally Fractured Reservoirs." Int. J. for Numerical and Analytical Methods in Geomech. **26**(5).

Sanyal, S. K., E. E. Granados, et al. (2005). An Alternative and Modular Approach to Enhanced Geothermal Systems. World Geothermal Congress 2005, Antalya, Turkey.

Sausse, J., Desayes, C. and Genter, A. (2007). "From geological interpretation and 3D modelling to the characterization of the deep seated EGS reservoir of Soultz (France)." Proceedings European Geothermal Congress 2007, Unterhaching, Germany, May 30-June 1, 2007.

Shaik, A. R., M. A. Aghighi, et al. (2008). "An Innovative reservoir simulator can Help Evaluate Hot Water Production for Economic Development of Australian Geothermal reservoirs." GRC Transactions **32**: 97-102.

Shaik, A.R., Koh, J., Rahman, S. S., Aghighi, M. A. and Tran, N. H., 2009. Design and evaluation of well placement and hydraulic stimulation for economical heat recovery from enhanced geothermal systems. GRC Annual Meeting October 4–7, 2009, conference proceedings.

Tran, N., Z. Chen, et al. (2007). "Characterizing and modelling of fractured reservoirs with object-oriented global optimization." Journal of Canadian Petroleum Technology **46**(3): 39-45.

Willis-Richards, J., K. Watanabe, et al. (1996). "Progress toward a stochastic rock mechanics model of engineered geothermal systems." J. Geophys. Res. **101**.

Zhou, X. X., Ghassemi, A. and Cheng, A. H.-D., 2009. A three-dimensional integral equation model for calculating poro- and thermoelastic stresses induced by cold water injection into a geothermal reservoir. Int. J. Numer. Anal. Meth. Geomech. 2009; 33,1613–1640

Figures and Tables

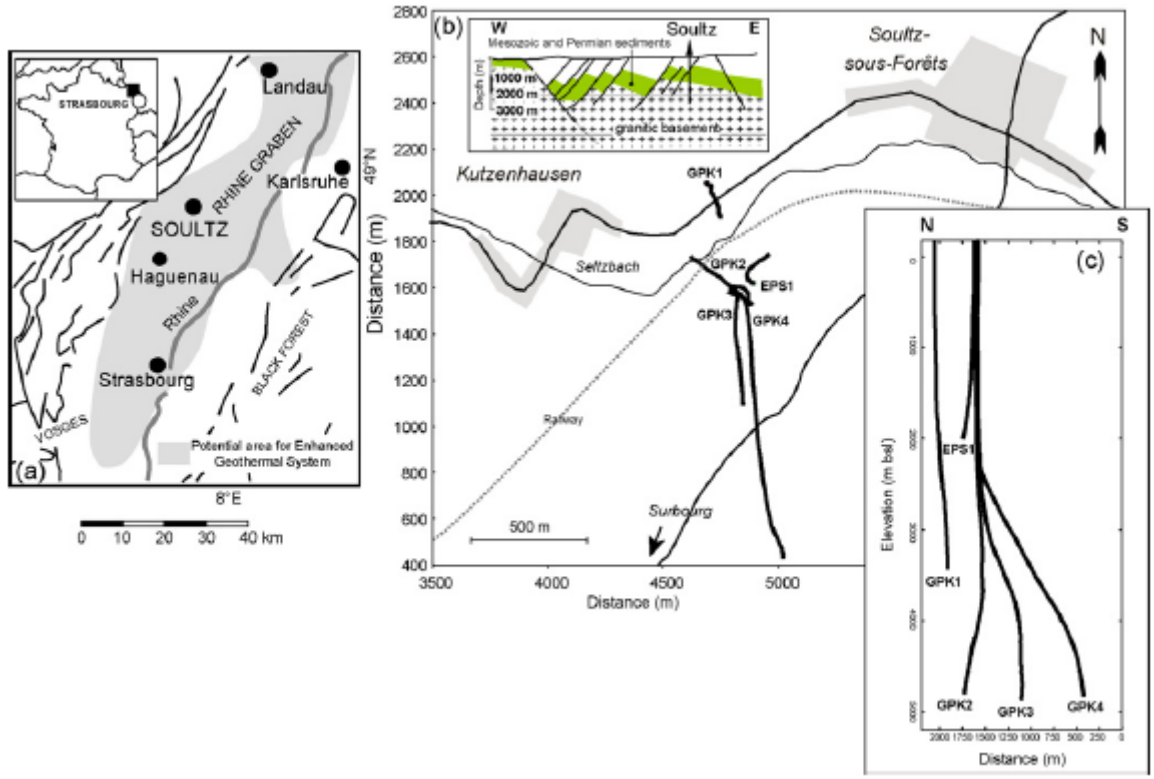

Fig. 1. Schematic geological map of the Rhine Graben and location of the Soultz-sous-Forets EGS site (a and b). Location and traces of the Soultz deep geothermal wells; solid lines correspond to well traces (b and c). (Sausse et al., 2006)

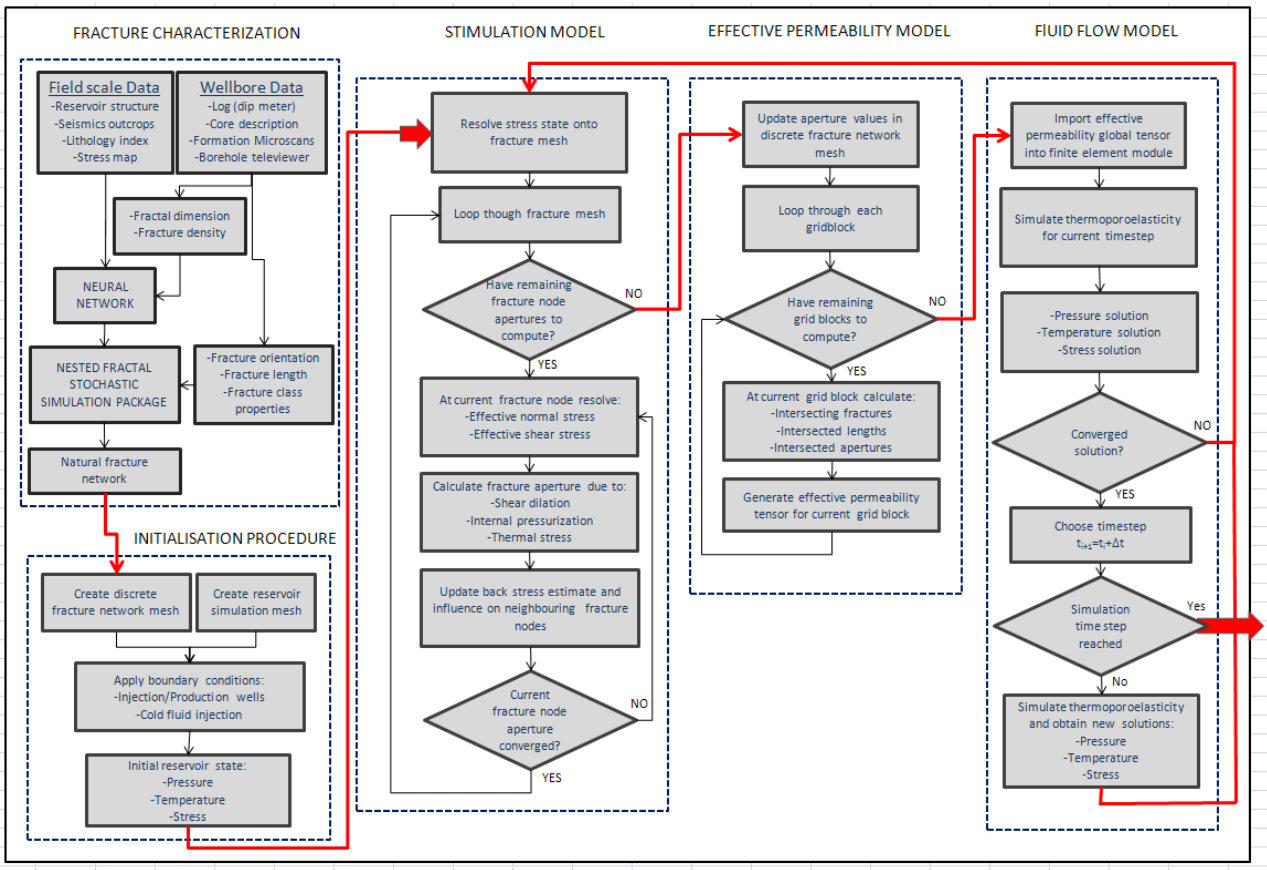

Fig 2. Flow chart describing the numerical procedure and integration between the various models.

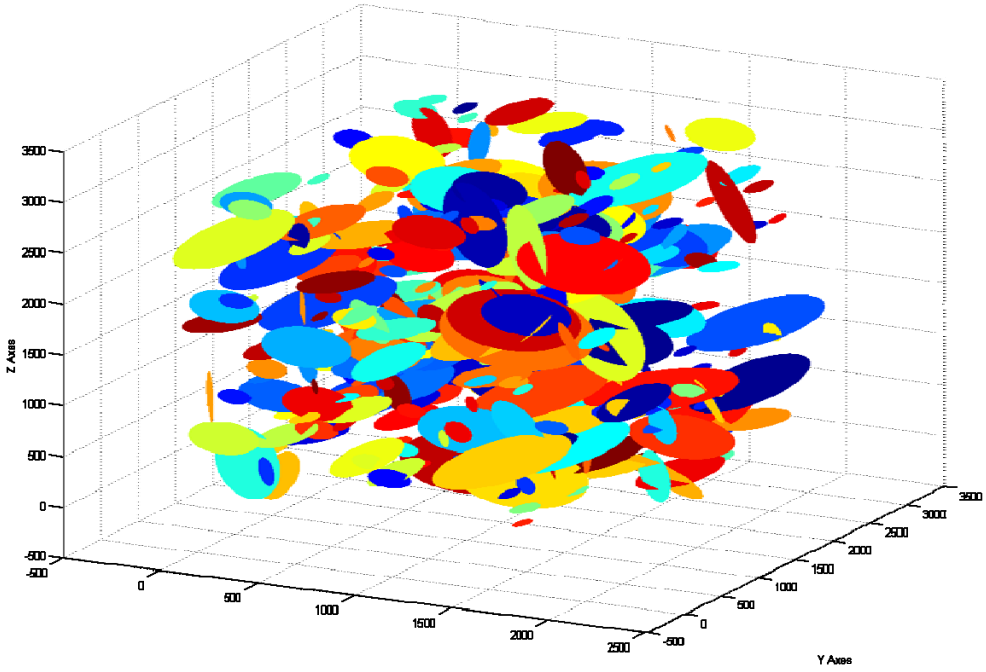

Fig. 3. Generated fracture network of the deep geothermal Soultz reservoir based on statistical data from Gentier et al. (2010).

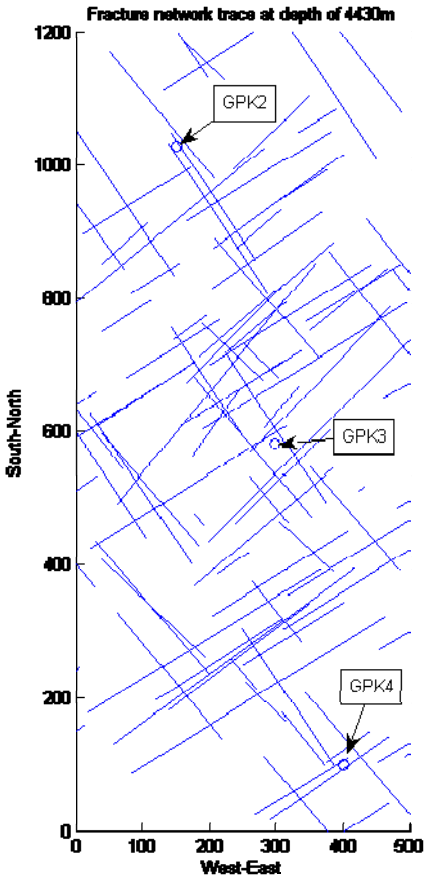

Fig. 4. A Soultz natural fracture network trace wells GPK2, GPK3 and GPK4 open holes at 4430 m. Trace plotted for fractures with radius greater than 60 m.

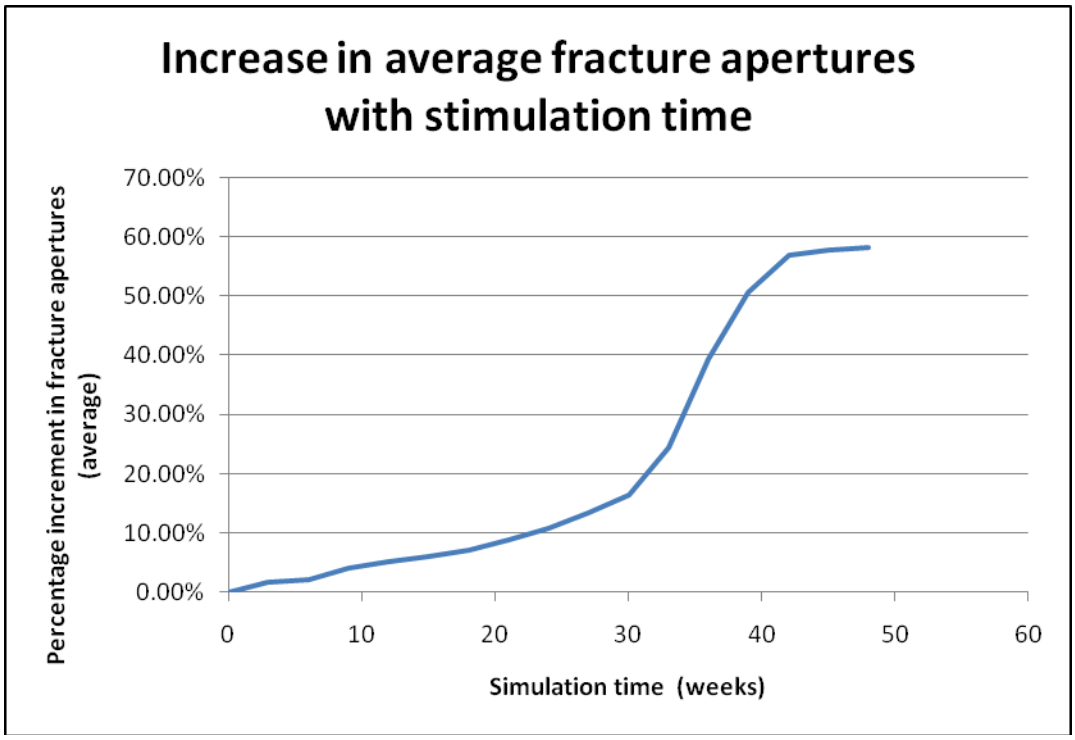

Fig. 5. Increase in average fracture aperture (retainable) with stimulation time. Injection pressure is 10,000 psi.

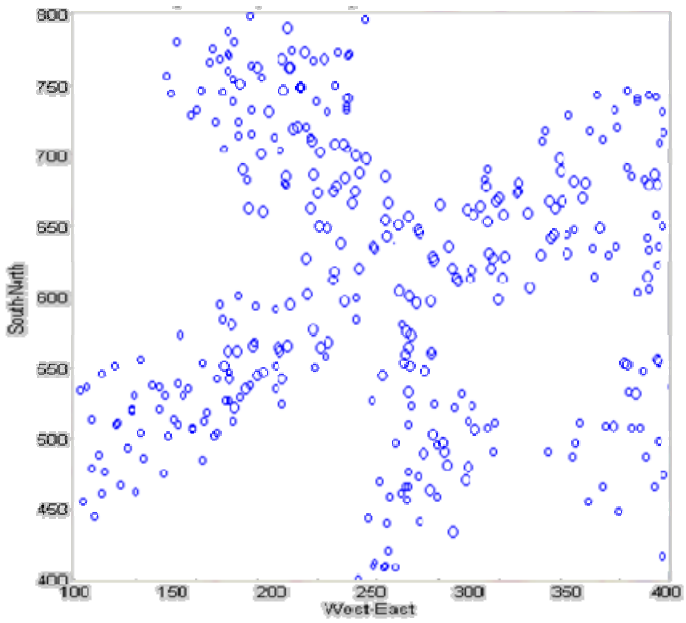

Fig. 6a. Cumulative shear dilation events in the fracture network after 8 weeks of stimulation (10,000 psi injection pressure) in a strike-slip stress regime. Marker sizes are proportional to the log of the event magnitudes.

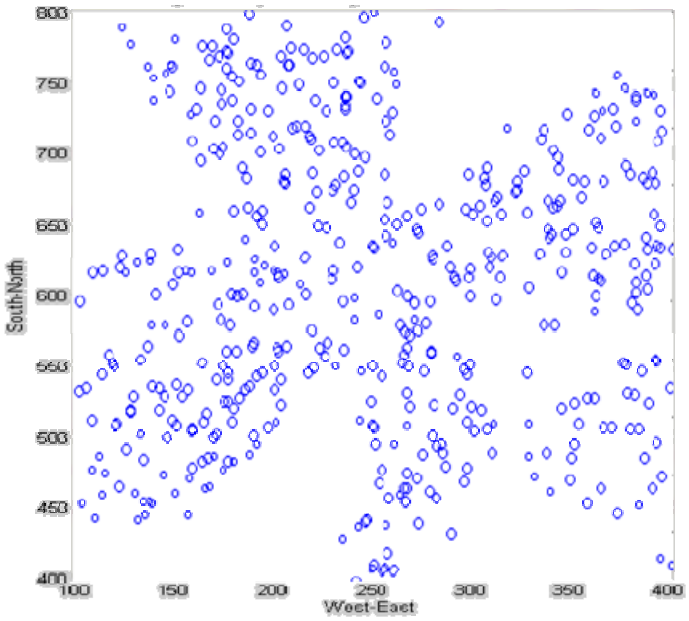

Fig. 6b. Cumulative shear dilation events in the fracture network after 24 weeks of stimulation (10,000 psi injection BHFP) in a strike-slip stress regime. Marker sizes are proportional to the log of the event magnitudes.

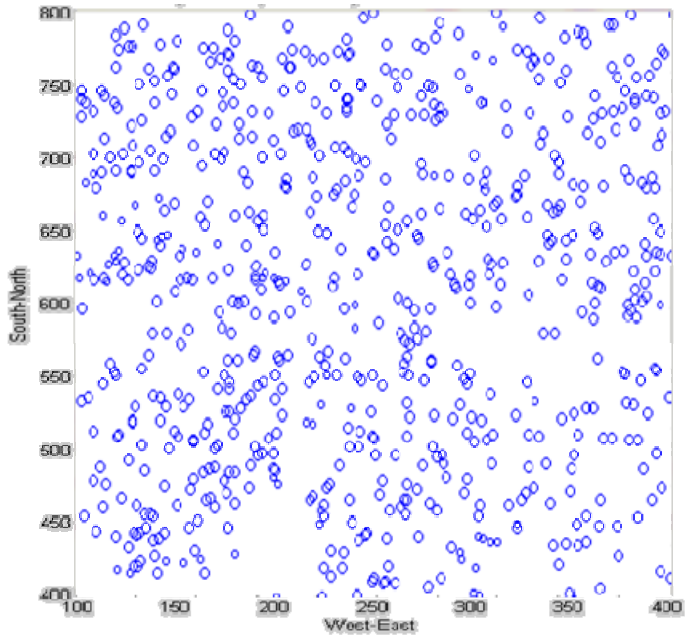

Fig. 6c. Cumulative shear dilation events in the fracture network after 40 weeks of stimulation (10,000 psi injection BHFP) in a strike-slip stress regime. Marker sizes are proportional to the log of the event magnitudes.

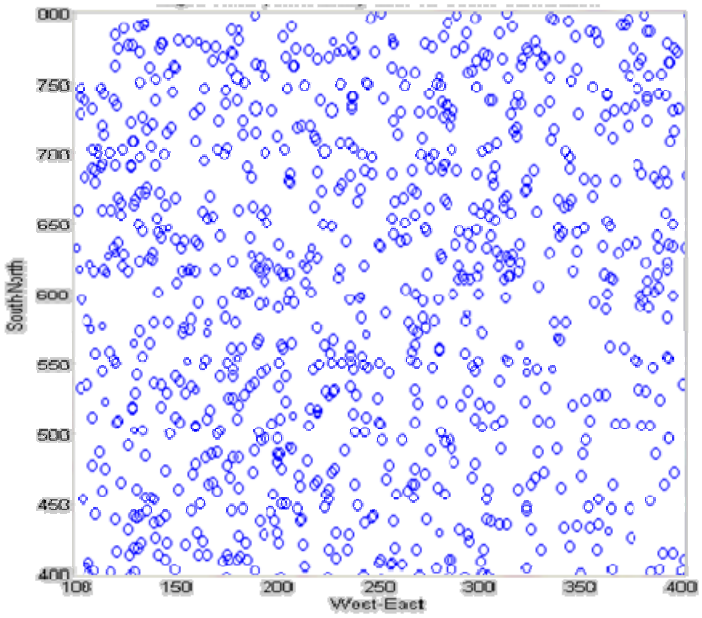

Fig. 6d. Cumulative shear dilation events in the fracture network after 52 weeks of stimulation (10,000 psi injection BHFP) in a strike-slip stress regime. Marker sizes are proportional to the log of the event magnitudes.

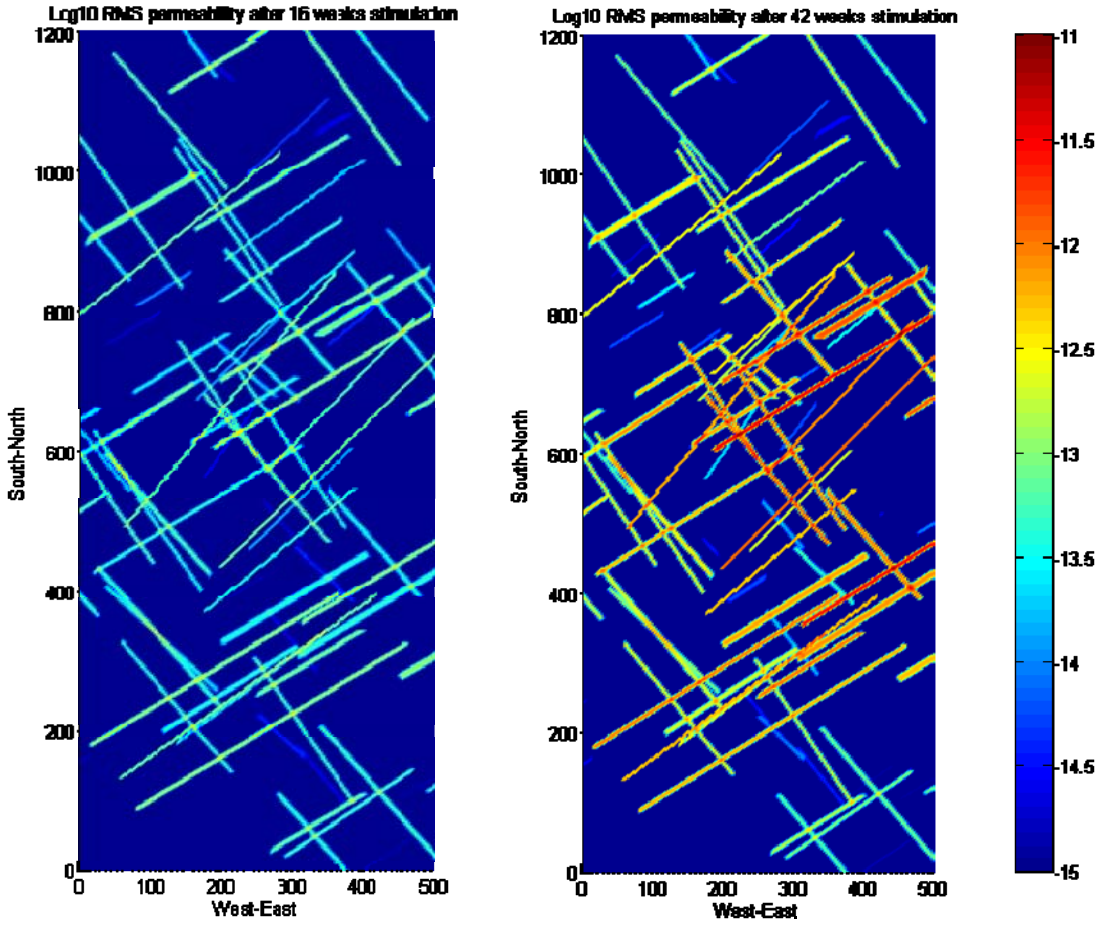

Fig. 7. Log_{10} RMS effective permeability profile (magnitudes of diagonal terms) after 16 weeks (left) and 42 weeks (right) of stimulation with 10,000 psi injection pressure, pre-production phase.

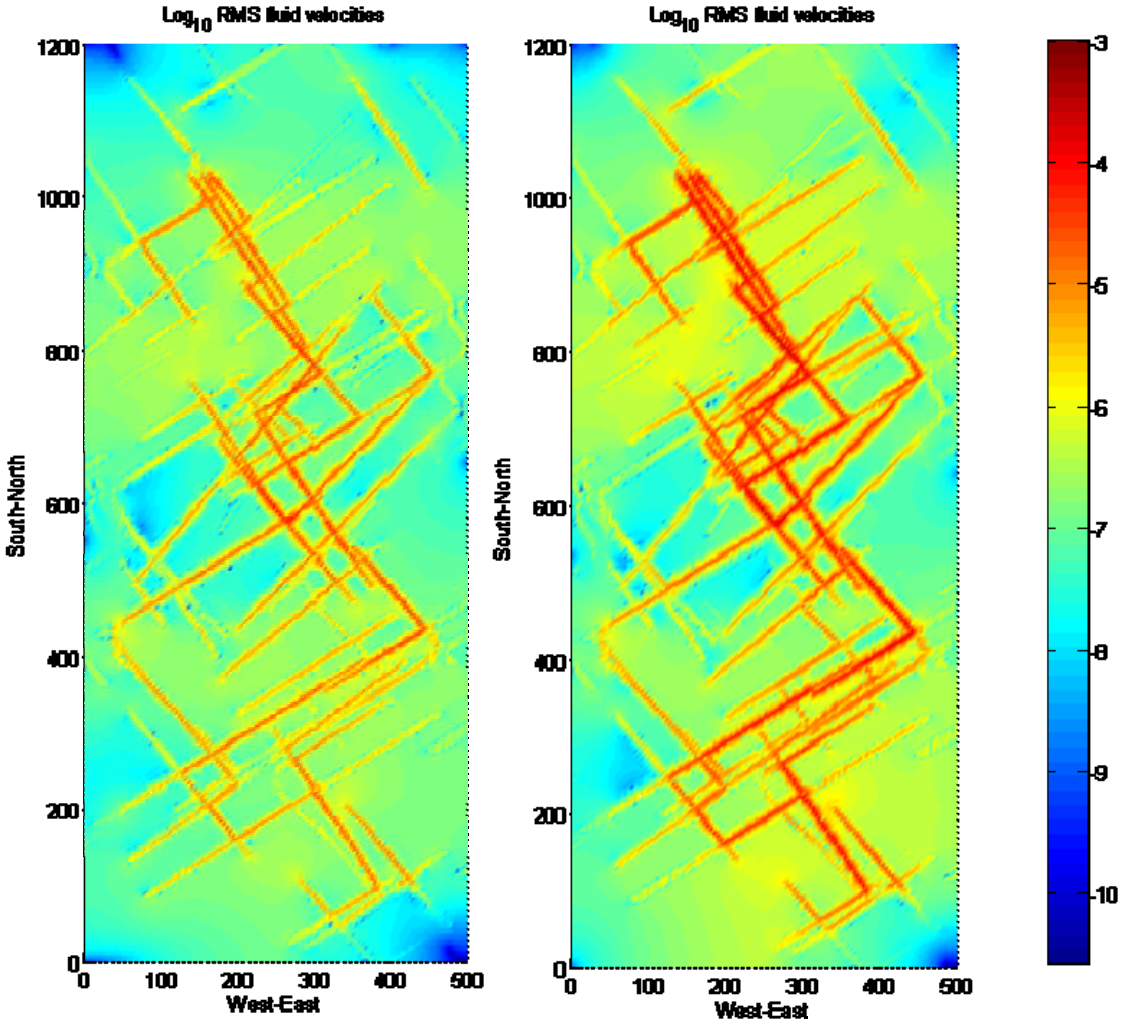

Fig. 8. Log_{10} fluid RMS velocity profiles (magnitudes) after 10 years production for injector-producer pressure drops of 2000 psi, stimulation time prior to running the production case was 16 weeks (left) and 42 weeks (right).

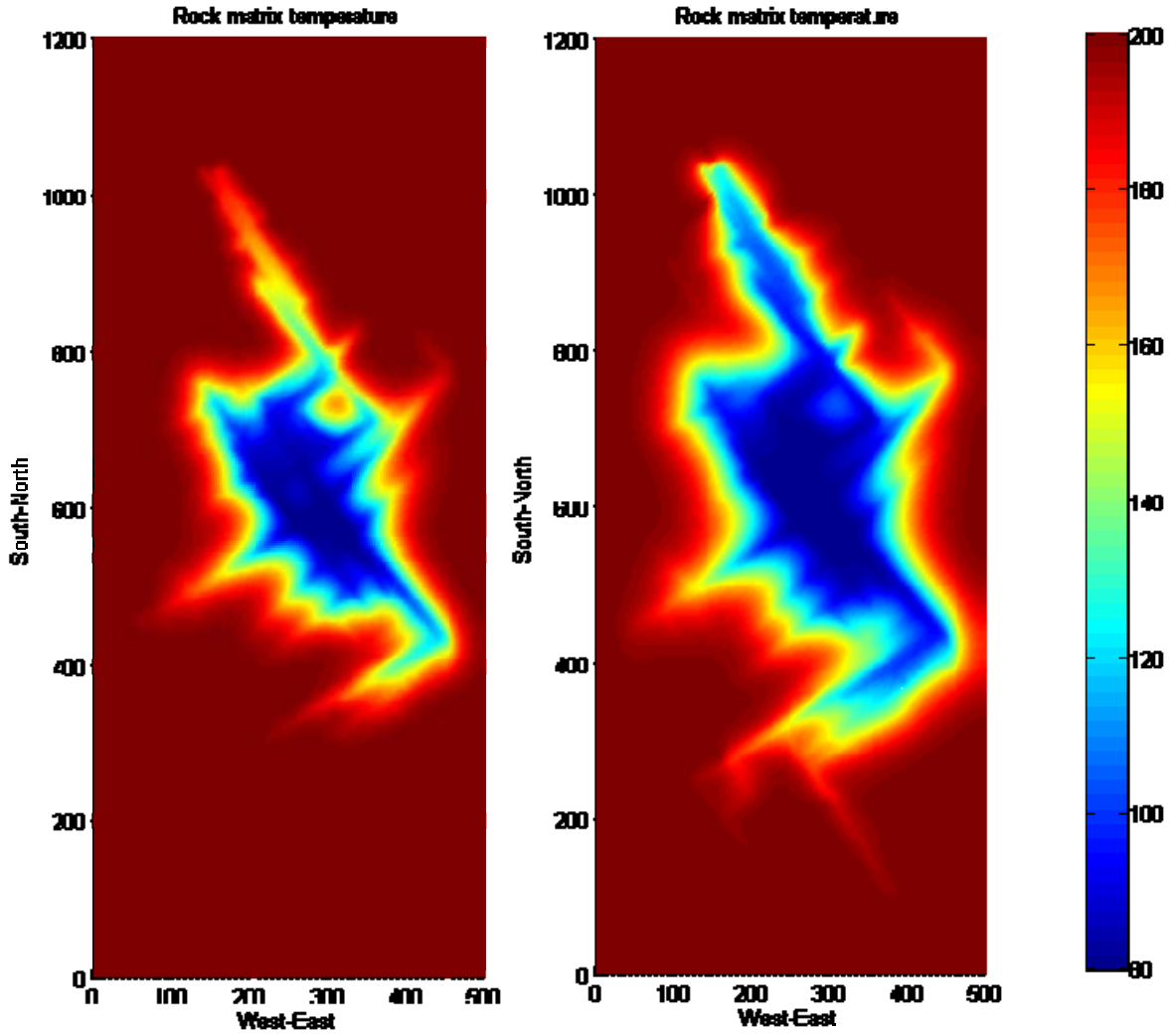

Fig. 9. Rock temperature profile after 10 years production for a injector-producer pressure drops of 2000 psi. Blue indicates rock at 80°C and red indicates rock at 200°C, stimulation time prior to running the production case was 16 weeks (left) and 42 weeks (right).

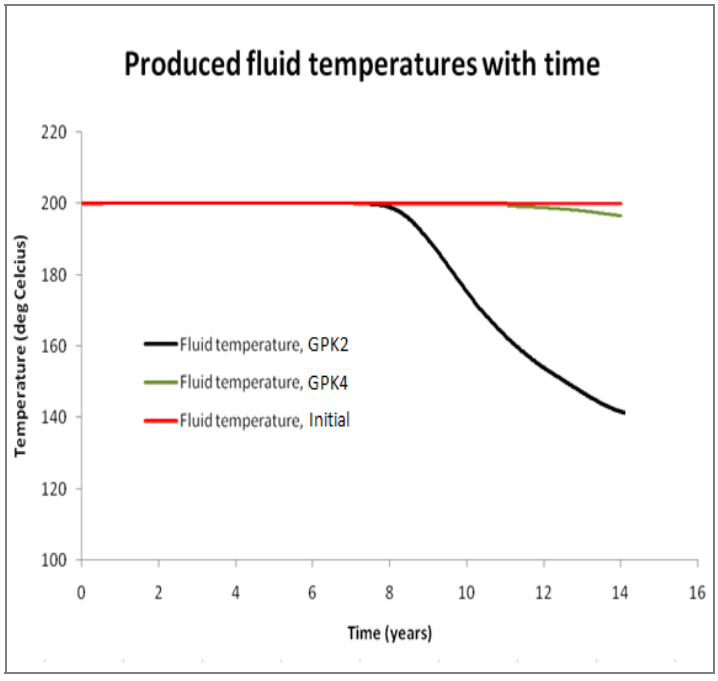

Fig. 10. Produced fluid temperatures vs. production time for GPK2 and GPK4. Stimulation time prior to running the production case was 42 weeks.

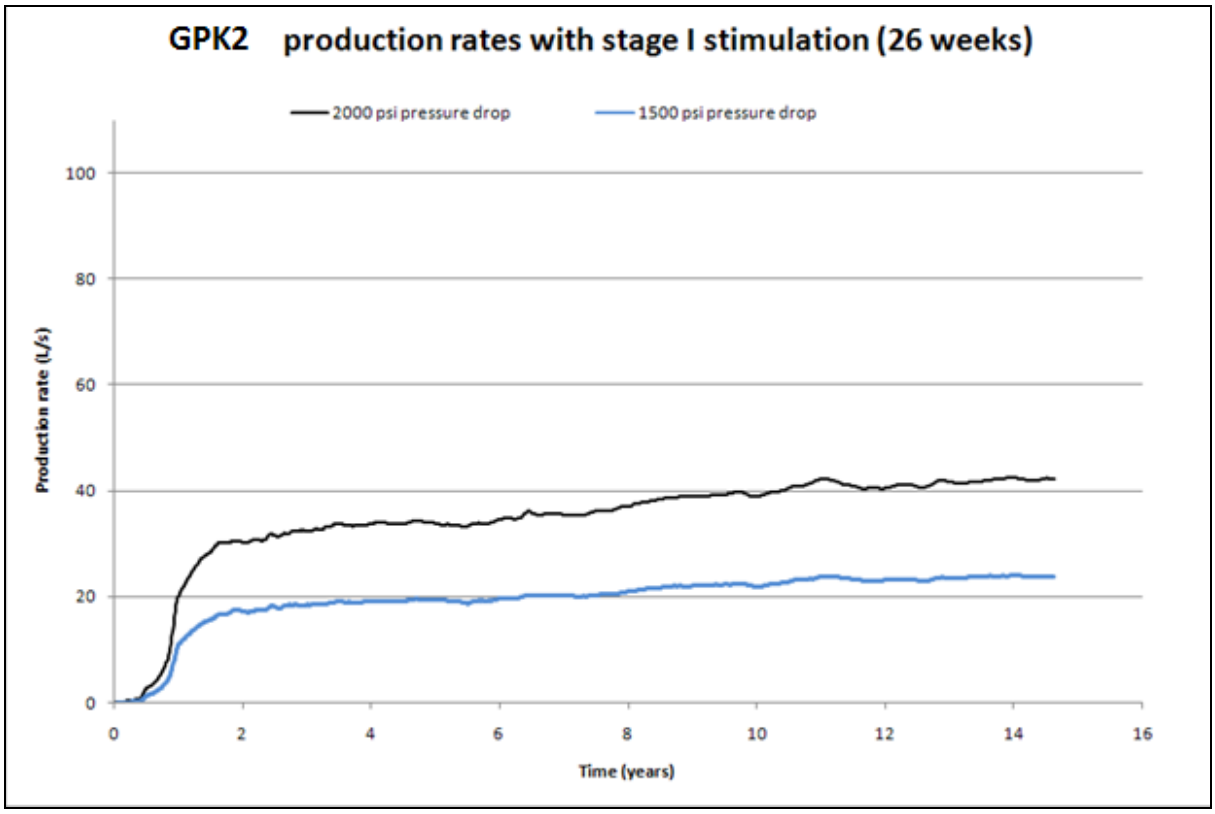

Fig. 11a. GPK2 production rates for injector-producer pressure drops of 2000 psi and 1500 psi over 15 years, with a reservoir stimulation time of 26 weeks.

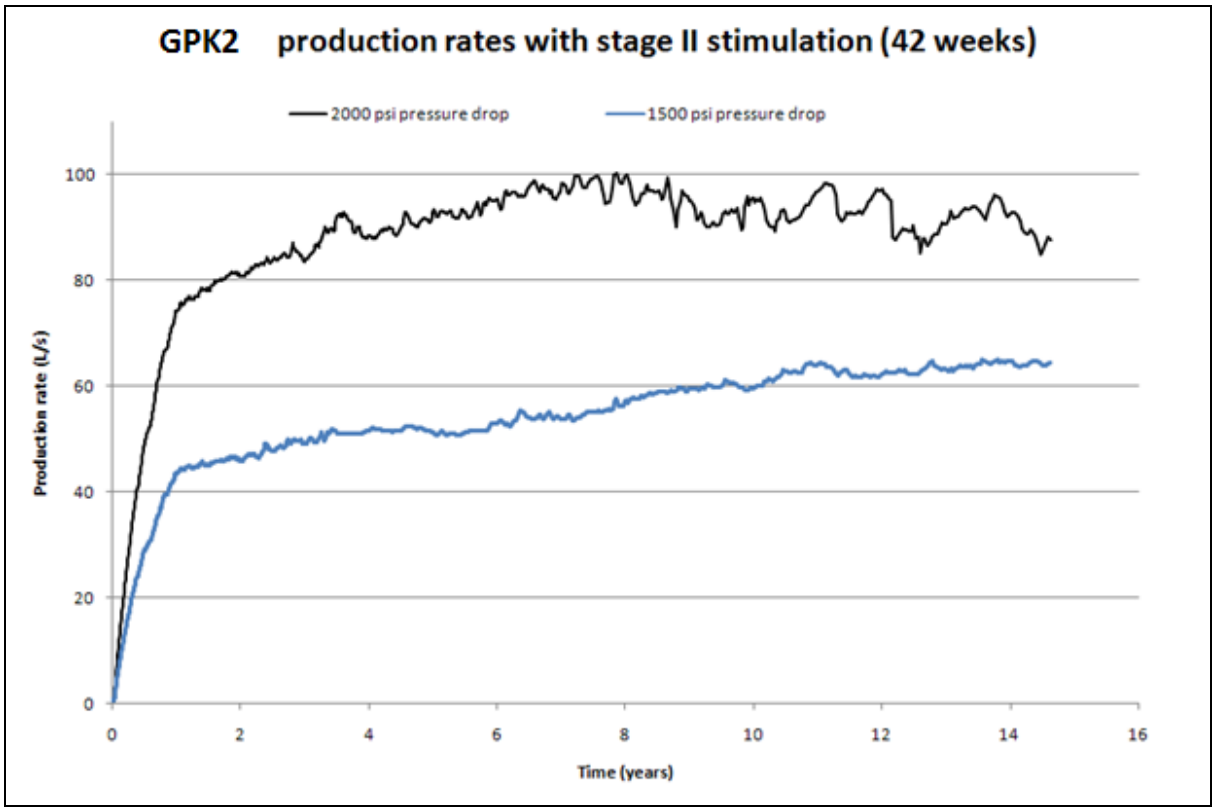

Fig. 11b. GPK2 production rates for injector-producer pressure drops of 2000 psi and 1500 psi over 15 years, with a reservoir stimulation time of 42 weeks.

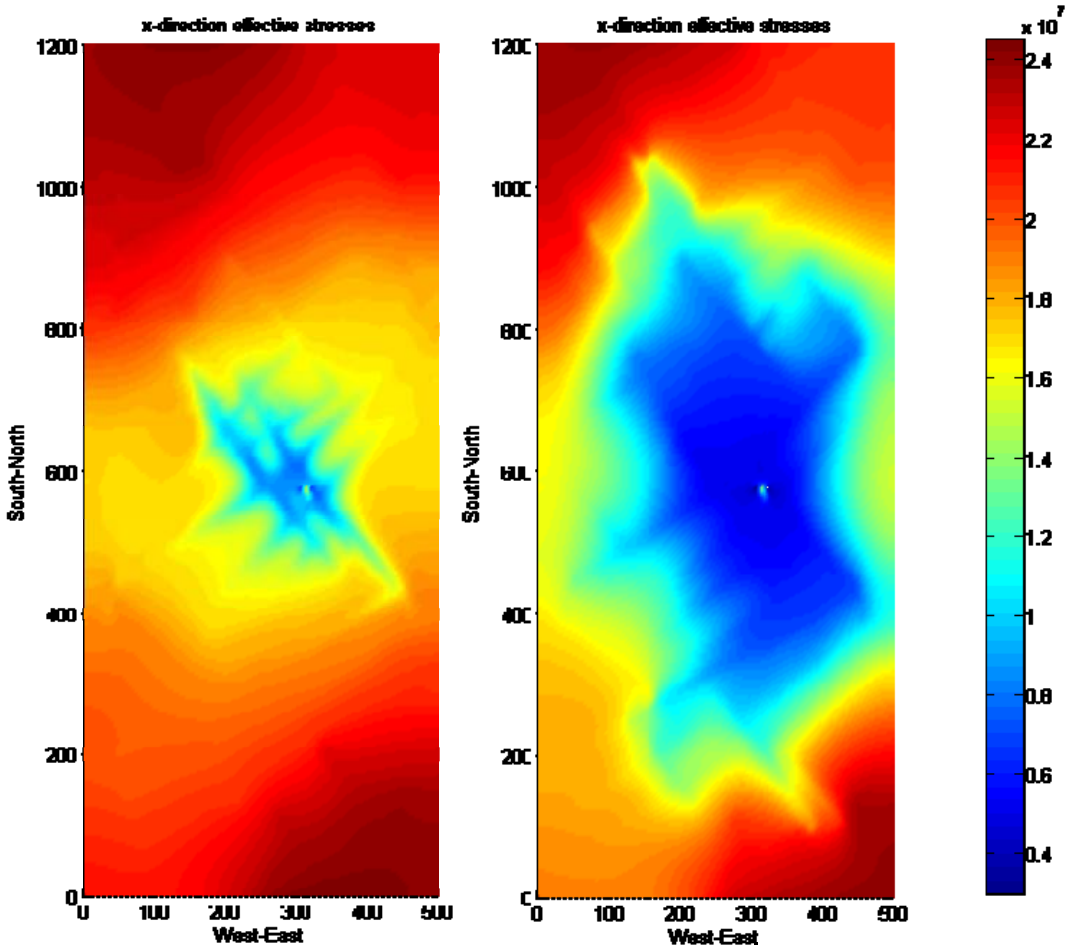

Fig. 12a. Effective stresses in the x direction at 3 years (left) and 10 years (right) injection time. Stimulation time prior to running the production case was 42 weeks.

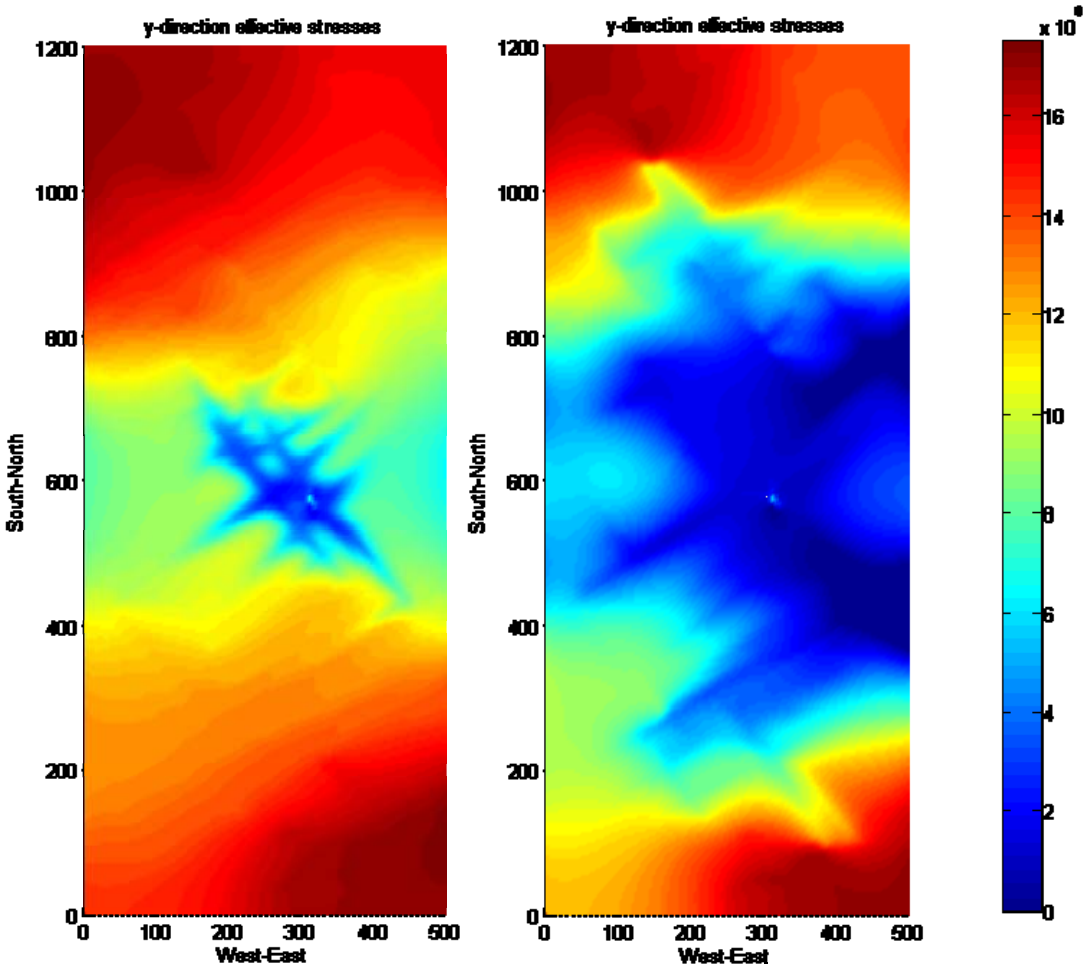

Fig. 12b. Effective stresses in the y direction at 3 years (left) and 10 years (right) injection time. Stimulation time prior to running the production case was 42 weeks.

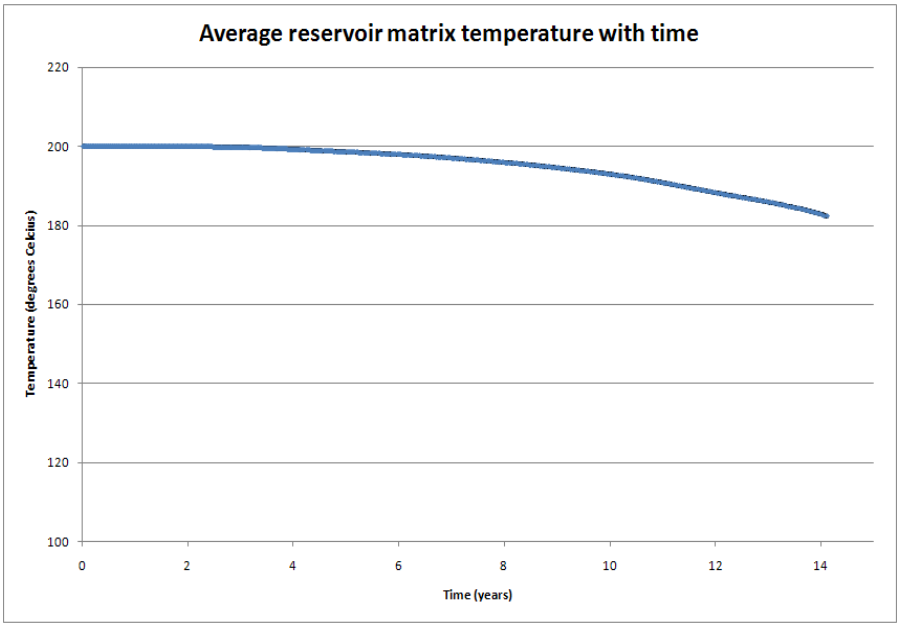

Fig. 13. Average matrix temperature vs. production time for 1.2 km (North-South) by 1.0 km (East-West) block enclosing wells GPK2, GPK3 and GPK4. Stimulation time prior to running the production case was 42 weeks.

Fracture set #	Plane direction			Dip				Number of fractures centers/m^3	Radius [m]	Transmissivity [m^4/s]
	Distribution law used	Mean	Half-width	Distribution law used	Mean	Half-width	Dip direction			
F1	Normal	2	16	Normal	70	7	NW	$1.30\ 10^{-7}$	187	$6.0\ 10^{-6}$
F2	Normal	162	19	Normal	70	7	NE	$3.00\ 10^{-9}$	150	$6.0\ 10^{-6}$
F3	Normal	42	6	Normal	74	3	NW	$1.76\ 10^{-8}$	95	$4.0\ 10^{-6}$
F4	Normal	129	6	Normal	68	3	SW	$3.30\ 10^{-8}$	112	$2.0\ 10^{-6}$
F5	Uniform	0	180	Normal	70	9	--	$1.00\ 10^{-8}$	100	$5.0\ 10^{-7}$

Table 1. Characteristics of statistical fracture sets obtained from Gentier et al. (2010). Plane direction is measured positive clockwise from North and dip positive downward from horizontal.

Rock Properties	
Young's modulus (GPa)	40
Poisson's ratio	0.25
Density (kg/m^3)	2700
Fracture basic friction angle (deg)	40
Shear dilation angle (deg)	2.8
90% closure stress (MPa)	20
In situ mean permeability (m^2)	9.0×10^{-17}
Fracture properties	
Fractal Dimension, D	1.2
Fracture density (m^2/m^3)	0.12
Smallest fracture radius (m)	15
Largest fracture radius (m)	250
Stress data	
Maximum horizontal stress (MPa)	53.3
Minimum horizontal stress (MPa)	78.9
Fluid properties	
Density (kg/m^3)	1000
Viscosity (Pa s)	3×10^{-4}
Hydrostatic fluid pressure (MPa)	34.5
Injector pressure, stimulation (MPa)	68.9
Injector pressure, production (MPa)	44.8
Producer pressure, stimulation	N/A
Producer pressure, production	31.0
Other reservoir data	
Well radius (m)	0.1
Number of injection wells	1
Number of production wells	2
Reservoir depth (m)	4430

Table 2. Stress and reservoir data for strike-slip stress regime.